

Modeling and experimental study of convective noise in electrochemical planar sensitive element of MET motion sensor

Vadim Agafonov^{a,*}, Anna Shabalina^a, Dongge Ma^b, Vladimir Krishtop^c

^a Moscow Institute of Physics and Technology (State University), Dolgoprudny, Russia

^b South China University of Technology, Guangzhou, PR China

^c Institute of Microelectronics Technology and High Purity Materials RAS, Chernogolovka, Russia



ARTICLE INFO

Article history:

Received 25 September 2018

Received in revised form 20 April 2019

Accepted 21 April 2019

Available online 7 May 2019

Keywords:

Electrochemical motion sensors

Self-noise

Hydrodynamics

Langevin method

Planar electrodes

ABSTRACT

The paper presents modeling and experimental study of the noise produced in planar sensitive element of electrochemical motion sensors. The experimental sample of the sensitive element has been produced using microelectronics methods. It has been manufactured as a narrow channel formed by two silicon plates with a set of electrodes placed on one of the plates. The channel is filled with water-based solution of potassium iodide with a small amount of iodine. In the end of the channel there are rubber membranes allowing the liquid to pass through the channel as the result of inertial forces associated with external motion. The liquid motion is converted into electrical response by the electrode system. The self-noise of the sample has been measured by comparing its output signals and output of the commercial low-noise seismometer, recorded side by side and followed by correlation analysis. The theoretical model uses equations of hydrodynamics and charge transfer in the concerned system. The stochastic behavior of the system is modeled by Langevin method applied to equations of hydrodynamics. The electrode current noise is calculated and is in a good agreement with the experimental data.

© 2019 Elsevier B.V. All rights reserved.

1. Introduction

MET (molecular electronic transfer) is a scientific and technological concept which uses an electrochemical cell as a basic signal converting element. It has resulted in the appearance of a new class of highly sensitive sensors of motion parameters, first of all, of short period and broadband seismometers, seismic accelerometers and angular motion sensors [1,2]. The developed devices are used in seismology [3–5], structural monitoring [6], navigation [7] broadband microseismic studies [8] and other areas.

At the same time, some of the problems associated with the fundamental nature of the processes occurring in electrochemical converting element still remain unsolved and that limits the possibility to improve the MET devices technical parameters and extend their usage. These problems include identification of nature and modeling of the sensors self-noise.

Among other mechanisms [9–11] the convective noise [12] is especially important for electrochemical sensors, since for many modifications of the sensors, such as accelerometers [13], angular motion sensors [14] and hydrophones [15], it dominates over other

types of noise in a wide frequency range. At the same time there is a lack of published researches providing both the experimental analysis of MET self-noise and theoretical modeling. Moreover, none of the researches combine modeling and experimental study for the same configuration of MET cell allowing to perform direct comparison of the experiments and theory, which is extremely important for verification of the basic assumptions on the fundamental nature of the MET self-noise.

Theoretical studies performed in this work are based on the speculation that the output current self-noise of transductive electrochemical element of MET sensor is conditioned by stochastic hydrodynamic flows in the working fluid. The studied cell geometry corresponds to the practical planar type transductive element with the electrode system spread on the surface, which is in contact with highly concentrated electrolyte solution [16,17].

To describe the mechanism of random currents appearance, the approach is based on the solution of Navier-Stokes hydrodynamics equations, where the right-hand side contains derivatives of random stress tensor with the known correlation functions [18,19]. The transformation of hydrodynamic flows into interelectrode electric current is described by the equation of convective diffusion with boundary conditions, which are the conditions of constant concentration of the active component of the working fluid on the electrodes and the absence of electric current through non-

* Corresponding author.

E-mail address: agafonov.vm@mpt.ru (V. Agafonov).

conductive surfaces. The analysis resulted in the expression for the power spectral density of electrical current fluctuations, the values of which at specific geometric parameters are calculated using numerical algorithms. At low frequencies, the frequency dependence of the noise power spectral density output is relatively weak, and then it increases reaching asymptotic dependence at the highest frequencies.

To verify experimentally the hypothesis of random hydrodynamic forces as a source of convective noise and the mathematical model developed to describe it, an experimental sample of the electrochemical cell with parameters similar to those used in the calculation has been manufactured and its noise has been measured experimentally. The experimental result is in good agreement with the theoretical prediction. In particular, at frequencies from 10 to 200 Hz, the data fit well the theoretically predicted dependence of $1/\omega^{1.5}$. The practical value of the developed model is to identify the physical mechanism responsible for the occurrence of the convective noise in MET sensor transduction element and in the ability to use the obtained knowledge and models in the development of the next generation of MET sensors.

2. Methods

2.1. Device physics and basic equations

The sensing element of the MET sensor is a system of microelectrodes placed in a thin channel filled with a working fluid which moves under the influence of inertial forces and is connected to the voltage source. A number of the cell configurations have been described in literature [20–24]. All reported cells comprise of two pairs of microelectrodes placed in the channel so that for any direction of inertial force, the liquid moves from the anode to the cathode in one pair of the electrodes and from the cathode to the anode in the other pair. The working solution is a highly concentrated aqueous iodide salt solution (usually potassium iodide is used) with a small amount of molecular iodine. In aqueous solution, iodide salt dissolves into positive K^+ and negative I^- ions. Iodine I_2 is present in the form of tri-iodide ions I_3^- . If voltage is applied between the electrodes, the following reversible electrochemical reaction takes place on the electrodes [9,25]:



The reaction proceeds from left to right on the anode and in the opposite direction on the cathode. Each elementary reaction is associated with the transfer of two electrons across the electrode surface. So, the electrical current can be determined if the flow of tri-iodide ions across the electrode is known. This fact is used in convective diffusion based model of charge transfer allow-

ing to consider the transfer of only ions I_3^- type, thus simplifying the mathematical problem. The I_3^- are referred to as active ions.

The transport of tri-iodide ions (called the active component) without electric migration is described by convective-diffusion equation:

$$\frac{\partial c}{\partial t} + D \Delta c = (\bar{v} \nabla c) \quad (2)$$

Here c denotes the ions I_3^- concentration and D denotes the diffusion coefficient. \bar{v} is the hydrodynamic velocity. For the Eq. (2), a simple boundary condition of the constant concentration on the electrodes is used in many studies [26–28].

The hydrodynamic velocity could be found from the Navier-Stokes linearized equation and incompressibility condition:

$$\frac{\partial \bar{v}}{\partial t} = \gamma \Delta \bar{v} - \Delta p / \rho + \bar{f} \\ \operatorname{div} \bar{v} = 0 \quad (3)$$

Here γ is the viscosity, p is the pressure, \bar{f} is the external volumetric force. The hydrodynamic velocity is zero on all rigid surfaces.

In case the concentration c is found, the density of the current due to electrochemical reactions (1) passing across the electrode surface could be calculated as follows:

$$j_{\text{anode}, \text{cathode}} = -2Dq \nabla c \cdot \mathbf{n} \Big|_{x \in \text{anode}, \text{cathode}} \quad (4)$$

Finally, the electrical current passing through the electrode could be determined by integrating (4) over the electrode surface. Usually, the changes of the cathodic current due to hydrodynamic velocity variations are used as a transducer output.

2.2. Experimental sample of the sensor with planar type electrochemical converting element

A sample of the planar sensitive element has been manufactured based on silicon technology by lift-off lithography method. A silicon plate 18 × 18 mm in size has been oxidized and platinum microelectrodes have been placed over the silicon oxide layer. The outline of the plate with the electrodes is shown in Fig. 1. As shown in the left part of Fig. 1, the central part is occupied by the electrode microstructure, while the side parts are used for external leads. The enlarged central part of the electrode structure is presented in the right part of Fig. 1. All electrodes are 20 μm wide. The electrodes are divided into two groups separated by 100 μm gap.

During the production process, a 100 mm diameter plate has been oxidized in a diffusion furnace at the depth of 0.25 μm, then an electronic lithographer has been used to perform electron-beam lithography over the plate, developing by immersing in a solvent and etching scrape in oxygen plasma. Next, the method of ion-plasma deposition has been used to apply a 60 nm platinum layer,

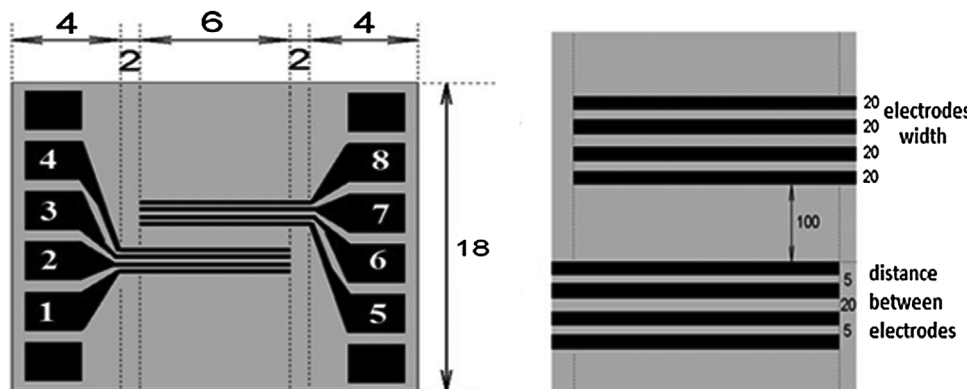


Fig. 1. The planar sensing cell sample. The entire sample is on the left, dimensions shown in millimeters. The central workspace with microelectrodes is on the right, the dimensions are in microns.

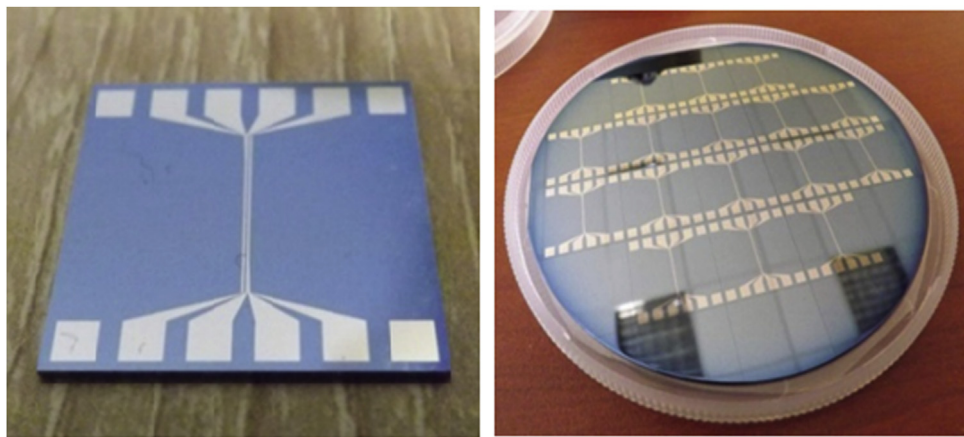


Fig. 2. The planar cell sample views. The sample is on the left, the plate with samples is on the right.

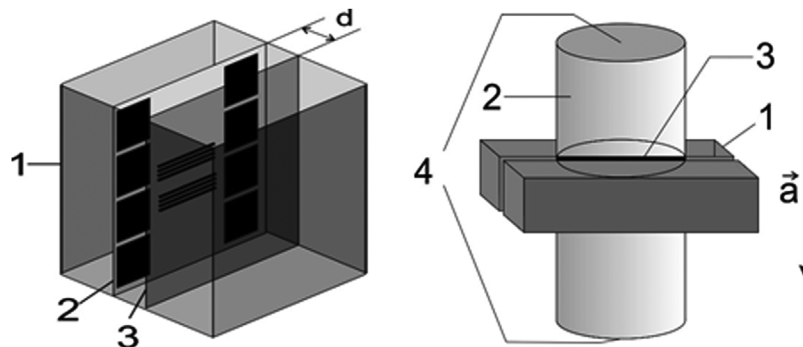


Fig. 3. Layout of the sensor with planar cell as a sensing element. Left - Unit with a planar cell: 1 - dielectric plate; 2 - planar cell; 3 - second dielectric plate. Right - the design of the sensor with a planar cell as a sensing element. 1 - unit with planar cell shown on the left; 2 - chamber filled with an electrolyte, 3 - gap with planar electrochemical cell; 4 - membranes.

together with an adhesive 7 nm sublayer of chromium. The selected method has allowed to quickly produce simple patterns with a single-layer topology without using expensive photomasks. The practical limit of the platinum film thickness in this method is up to 100 nm, in contrast to the photolithography and the electron beam evaporation techniques, where the platinum microstructures layer thickness can be up to 300 nm [15]. For the purposes of this study, these technological limitations are not significant. The actual view of the plates with the electrode structure is presented in Fig. 2.

Then the produced planar cell was glued on one of the two insulating plates which were arranged parallel to each other so that the gap between the planar cell and the second plate was 100 μm (Fig. 3, left). The produced unit with a glued-in planar cell was placed in a cylindrical dielectric housing with flexible membranes at the ends, so that the gap between the planar cell and the second plate was the only channel connecting the lower and the upper parts of the housing volume (Fig. 3, left). The housing was filled with 4 mol/l KI water-based electrolyte solution with the additive of active iodine $c_0 = 0.01 \text{ mol/l}$ (Fig. 3, right).

Chemically resistant plastic with low iodine adsorption has been used in the manufacturing of the case. The experimental planar cell on dielectric surfaces has been coated with silicon oxide, which is also chemically resistant to iodine-iodide electrolyte and has low adsorption of the electrolyte components. Before the measurements, gas bubbles have been removed from the sensor volume using ultrasound and dynamic adiabatic degassing. This ensures stable operation of the sensor and eliminates bubble-caused sensor output instability.

If vertical acceleration is applied to the described sample, the inertial force produces liquid flow in the gap of the unit, changing

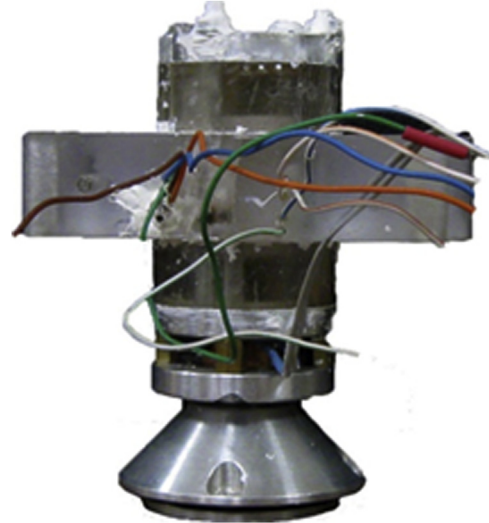


Fig. 4. Sensor assembly on a solid foundation. The calibration coil and the magnet attached to the membrane are placed in the lower part of the assembly.

the interelectrode currents. So, the produced sample works as a MET sensor equipped with a planar sensing unit. Additionally, the experimental sample has been equipped with a calibration coil and a magnet used to study sensors response. The actual view of the experimental MET sensor is shown in Fig. 4.

In the experiments, four electrodes of the cell are connected to the external electronics. The electronics produce a voltage bias of

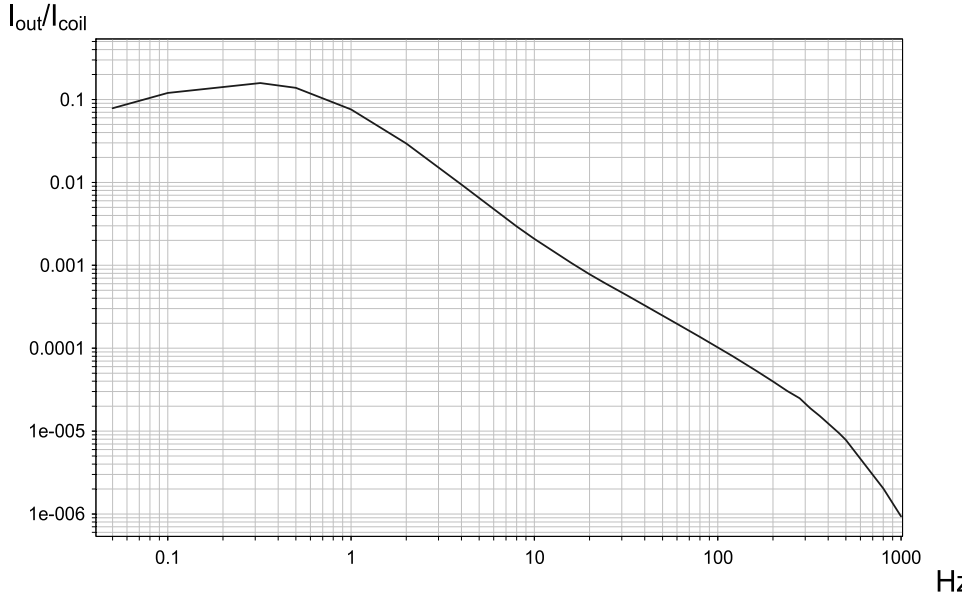


Fig. 5. Amplitude vs frequency response of the experimental sample.

300 mV between the electrodes in every pair and convert the electrode currents into output voltages. In the presented experiments, an ACCA connection method [28,29] has been used, so that the anodes are the external electrodes of the cell while the cathodes are the internal ones. In the experiments, two electrodes from the first group and two electrodes from the second group have always been used as anode-cathode pairs. The preliminary tests have shown that due to the large distance between the groups of electrodes the results almost do not depend on the specific electrodes from the groups used in the connection, so that all the following results are obtained for the configuration with the electrodes # 2 and #7 used as anodes of the cell, while the electrodes #3 and #6 are used as cathodes (Fig. 1).

Besides the bias source, the electronics include current-to-voltage converter, as described in [1,12] and high resolution A-to-D converter. The resulting output has been converted into the difference of the cathodic current variations using the known conversion coefficient of the electronics.

To check the cell performance, the amplitude-frequency response of the sensor has been obtained with a calibration coil, which impacted a magnet fixed to the lower flexible membrane. The impact was performed by preassigned harmonic current variations in the coil in the range of 0.5–1,000 Hz. The ratio of the output current to the input current in the coil at the frequencies of the input actions has been calculated (Fig. 5). Note that according to

[30] and [31], the obtained curve coincides within the accuracy of the coefficient with the amplitude characteristic of the acceleration sensor W_A : $W_I = K_A W_A$. The pre-measured coefficient value was $5500 \frac{m}{(A \cdot s^2)}$. The shape of the curve is typical for the electrochemical motion sensors [23,31].

2.3. Theoretical model

To specify a mathematical model according to the experimental sample configuration, consider a thin plane channel with electrodes deposited on one of the channel walls. Due to the large distance between the anode-cathode pairs, consider only one pair of anode/cathode electrodes. Both anode and cathode have the same width b and are separated by the distance a . d denotes the thickness of the channel. As shown in Fig. 6, let us introduce the coordinate system which starts on the surface, containing electrodes so that the anode and the cathode are placed symmetrically relative to the coordinate starting point. Direct X along the channel, Z is perpendicular to the channel walls, axis Y forms the right-hand coordinate system. The cell size in Y direction will be considered large in comparison with other sizes of the cell.

Consider Navier-Stokes and continuity equation for the incompressible liquid with stochastic Langevin force in the right part of Navier-Stokes Eq. (3) [29] $f_i = \partial S_{ij}/\partial x_j$, $i, j = x, y, z$. S_{ij} is the stress tensor. Also, take into account that in the experimental sample, the

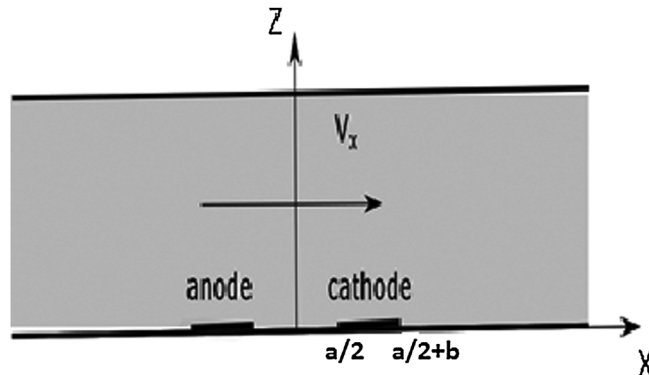


Fig. 6. Chart of planar MET cell.

channel length is large compared to the channel. Under these terms [18,30], the flow could be assumed unidirectional along the channel axis and $\partial^2 v_x / \partial z^2 >> \partial^2 v_x / \partial x^2, \partial^2 v_x / \partial y^2$:

$$\begin{aligned} \partial^2 v_x / \partial z^2 &= \partial S_{xz} / \partial z + \partial S_{xy} / \partial y + \partial S_{xx} / \partial x - 1/\rho \partial P / \partial x \\ \partial v_x / \partial x &= 0 \end{aligned} \quad (5)$$

The components of the stress tensors S_{xz}, S_{xy}, S_{xz} are uncorrelated between each other, and therefore, their contributions to the hydrodynamic velocity fluctuations can be regarded independent from each other. As discussed in [18], the first summand in (5) dominates in thin channels and the other terms can be disregarded.

Next, integrate Eq. (5) over x and over y . Introduce averaged stress and velocity according to the following: $\sigma_{xz} = \int_{-l/2}^{l/2} dx \int_{-s/2}^{s/2} S_{xz} dy$,

$$V_x = \int_{-s/2}^{s/2} v_x dy$$

After that the averaged velocity, which satisfies the slip boundary condition on the channel walls is written as:

$$V_x = \frac{1}{lv} \left(\int_0^z \sigma_{xz}(\tau) d\tau - \frac{z}{d} \int_0^d \sigma_{xz}(\tau) d\tau \right) + \frac{zs\Delta P}{2l\rho v} (d-z) \quad (6)$$

Determine the pressure difference ΔP across the channel from the condition of zero integral flow across the channel cross-section. Finally, use the formula $\langle S_{xz}(x, y, z) S_{xz}(x_1, y_1, z_1) \rangle = 2\nu\rho T \delta(x - x_1) \delta(y - y_1) \delta(z - z_1)$ [30,29] and result in the following:

$$\langle V_x(z) V_x(z_1) \rangle = \frac{2Ts}{\gamma\rho l} \left[\min(z, z_1) - \frac{zz_1}{d} - 3 \frac{zz_1}{d^3} (d-z)(d-z_1) \right] \quad (7)$$

Now consider the convective transfer of the active solution component (2). Seek the solution in the approximation of a small hydrodynamic velocity:

$$c = c_0 + c_{st} + c_1 \quad (8)$$

Here c_0 denotes the equilibrium concentration of the active component, c_{st} denotes the concentration deviation from the equilibrium concentration in stationary liquid in the presence of only diffusion carriers transfer, c_1 denotes the convective additive to the concentration, linear in hydrodynamic velocity. The terms proportional to higher powers of the hydrodynamic velocity have been omitted. Due to the cell geometry c_{st} does not depend on y coordinate and we can look at the averaged c_1 over y direction.

Then after the Fourier transform by x coordinate, obtain the following system:

$$\begin{aligned} \partial^2 c_{st} / \partial z^2 - k^2 c_{st} &= 0 \\ \partial^2 c_1 / \partial z^2 - (k^2 + i\omega/D)c_1 &= L(k, z) \\ L(k, z) &= -iV_x(z)kc_{st}(k, z)/D \end{aligned} \quad (9)$$

The solution of (9) can be shown as follows:

$$c_{st}(k, z) = \frac{\cosh k(d-z)}{\sinh kd} \frac{j_0(k)}{2Dqk} \quad (10)$$

$$\begin{aligned} c_1(k, z) &= \frac{j_1(k)}{2Dq\lambda} \frac{\cosh \lambda(d-z)}{\sinh \lambda d} + \frac{1}{\lambda} \int_0^z L(k, \zeta) \sinh(\lambda z - \lambda \zeta) d\zeta - \\ &- \frac{\cosh \lambda z}{\lambda \sinh(\lambda d)} \int_0^d L(k, \zeta) \cosh(\lambda d - \lambda \zeta) d\zeta \end{aligned} \quad (11)$$

Here $\lambda^2 = k^2 - \frac{i\omega}{D}$, $Re\lambda > 0$. $j_{0,1}(k) = \frac{1}{2\pi} \int_{S_{el}} j_{0,1}(\xi) e^{-ik\xi} d\xi$. Here $j_{0,1}(\xi)$ is the electrical current density on the electrodes. Index 0 corresponds to the stationary current and index 1 corresponds to the additive to the electrical current density linear in the velocity: $j_{0,1}(x) = -2Dq \partial c_{0,1} / \partial z |_{z=0} S_{el}$ index below the integral sign means integration over the surface of all the electrodes of the transducing system. To find the unknown distributions of the densities of the electric currents $j_{0,1}(\xi)$, take $z = 0$ in (10), (11) and perform the inverse Fourier transform:

$$\frac{1}{2\pi} \frac{1}{2Dq} \int_{-\infty}^{+\infty} dk \int_{S_{el}} \frac{\cosh kd}{\sinh kd} \frac{j_0(\xi)}{k} e^{ik(x-\xi)} d\xi = \begin{cases} -c_0, x \text{ecathode} \\ c_0, x \text{eanode} \end{cases} \quad (12)$$

$$\begin{aligned} &\int_{-\infty}^{+\infty} dk \int_{S_{el}} \frac{j_1(\xi)}{\lambda} \frac{\cosh(\lambda d)}{\sinh(\lambda d)} e^{ik(x-\xi)} d\xi = \frac{i}{D} \int_{-\infty}^{+\infty} dk \frac{1}{\lambda \sinh(\lambda d) \sinh kd} x \in S_e \\ &\times \int_{S_{el}} j_0(\xi) e^{ik(x-\xi)} d\xi \int_0^d V_x(\zeta) \cosh k(d-\zeta) \cosh \lambda(d-\zeta) d\zeta \end{aligned} \quad (13)$$

Due to the symmetry of the system consider $j_0(-\xi) = -j_0(\xi)$, $j_1(-\xi) = j_1(\xi)$ and go over to dimensionless numbers: $\tilde{d} = d/b$; $\tilde{a} = a/b; \tilde{x}, \tilde{\xi} = x, \xi, \zeta/b; \tilde{k} = kb; \tilde{\lambda} = \sqrt{\tilde{k}^2 - i\tilde{\omega}}$; $\tilde{\omega} = b^2\omega/D, \tilde{j}(\tilde{x}) = j(x)a/\pi Dqc_0, \tilde{V}_x = V_x b/D$. Then the Eq. (12) result in the following:

$$\frac{2}{\pi\tilde{a}} \int_0^{+\infty} \frac{\cosh \tilde{k}\tilde{d}}{\sinh \tilde{k}\tilde{d}} \frac{\sin \tilde{k}\tilde{x}}{\tilde{k}} \int_{\tilde{a}/2}^{\tilde{a}/2+1} \tilde{j}_0(\tilde{\xi}) \cdot \sin \tilde{k}\tilde{\xi} \cdot d\tilde{\xi} d\tilde{k} = -1 \quad (14)$$

$$\begin{aligned} &\int_0^{\infty} \frac{\cos \tilde{k}\tilde{x}}{\tilde{\lambda}} \frac{\cosh(\tilde{\lambda}\tilde{d})}{\sinh(\tilde{\lambda}\tilde{d})} d\tilde{k} \int_{\tilde{a}/2}^{1+\tilde{a}/2} \tilde{j}_1(\tilde{\xi}) \cos \tilde{k}\tilde{\xi} d\tilde{\xi} = \\ &= \int_0^{+\infty} d\tilde{k} \frac{\cos \tilde{k}\tilde{x}}{\tilde{\lambda} \sinh(\tilde{\lambda}\tilde{d}) \sinh \tilde{k}\tilde{d}} \int_{\tilde{a}/2}^{1+\tilde{a}/2} \tilde{j}_0(\tilde{\xi}) \sin \tilde{k}\tilde{\xi} d\tilde{\xi} \int_0^{\tilde{d}} \tilde{V}_x(\tilde{\zeta}) \cosh \tilde{k}(\tilde{d}-\tilde{\zeta}) \cosh \tilde{\lambda}(\tilde{d}-\tilde{\zeta}) d\tilde{\zeta} \end{aligned} \quad (15)$$

Here $\tilde{x} \in [\tilde{a}/2; \tilde{a}/2 + 1]$. To solve the integral Eq. (15), split the electrode surface into equal segments and present the current densities as follows:

$$\tilde{j}_0(\tilde{\xi}) = \sum_{n=1}^N A_n (\Theta(\tilde{\xi} - \tilde{x}_n - \frac{1}{2N}) - \Theta(\tilde{\xi} - \tilde{x}_n + \frac{1}{2N})) \quad (16)$$

$$\tilde{j}_1(\tilde{\xi}) = \sum_{n=1}^N B_n (\Theta(\tilde{\xi} - \tilde{x}_n - \frac{1}{2N}) - \Theta(\tilde{\xi} - \tilde{x}_n + \frac{1}{2N}))$$

and consider (14), (15) for discrete values of a variable $\tilde{x} = \tilde{a}/2 + (2l-1)/2N \equiv \tilde{a}/2 + \tilde{x}_l, l = 1\dots N$. Then obtain the following system of matrix equations:

$$\begin{aligned} \sum_{n=1}^N A_n M_{nl} &= -\tilde{a} \\ M_{nl} &= \int_0^{+\infty} \frac{\cosh \tilde{k}\tilde{d}}{\sinh \tilde{k}\tilde{d}} \frac{\sin \tilde{k}(\frac{\tilde{a}}{2} + \tilde{x}_l) \sin \frac{\tilde{k}}{2N} \sin \tilde{k}(\frac{\tilde{a}}{2} + \tilde{x}_n)}{\tilde{k}^2} d\tilde{k} \end{aligned} \quad (17)$$

$$\sum_{m=1}^N B_m K_{ml} = R_l$$

$$R_l = \int_0^{+\infty} d\tilde{k} \frac{\cos \tilde{k}(\frac{\tilde{a}}{2} + \tilde{x}_l)}{\tilde{\lambda} \sinh(\tilde{\lambda}\tilde{d}) \sinh \tilde{k}\tilde{d}} \frac{2}{\tilde{k}} \sin \frac{\tilde{k}}{2N} \sum_{n=1}^N A_n \sin \tilde{k} \left(\frac{\tilde{a}}{2} + \tilde{x}_n \right) \times$$

$$\times \int_0^{\tilde{d}} \tilde{V}_x(\tilde{\xi}) \cosh \tilde{k}(\tilde{d} - \tilde{\xi}) \cosh \tilde{\lambda}(\tilde{d} - \tilde{\xi}) d\tilde{\xi}$$

$$K_{ml} = \int_0^{+\infty} \frac{2 \cos \tilde{k}(\frac{\tilde{a}}{2} + \tilde{x}_m) \cdot \cos \tilde{k}(\frac{\tilde{a}}{2} + \tilde{\xi}_l)}{\tilde{\lambda} \tilde{k}} \frac{\cosh \tilde{\lambda} \tilde{d}}{\sinh \tilde{\lambda} \tilde{d}} \sin \frac{\tilde{k}}{2N} d\tilde{k}$$
(18)

The solution of (17), (18) write through the matrices reciprocal to $|M|$ and $|K|$:

$$A_n = -\tilde{a} \sum_{l=1}^N M_{nl}^{-1}$$
(19)

$$B_m = \sum_{l=1}^N R_l K_{lm}^{-1}$$
(20)

Then the total current flowing through the electrode, which is linear in the hydrodynamic velocity, can be represented as follows:

$$\tilde{I}_1 = \sum_{m=1}^N B_m = \sum_{l=1}^N R_l K_l^{-1}$$
(21)

Where $K_l^{-1} = \sum_{m=1}^N K_{ml}^{-1}$ and in subsequent calculations can be obtained from the solution of:

$$\sum_{l=1}^N K_{nl} K_l^{-1} = 1, n = 1 \dots N$$
(22)

For random flows, the velocity distribution is unknown, however, the correlation function (7) is known. Then the expression for the spectral density of current fluctuations through the electrode surface has the following form:

$$\langle I_{\omega}^2 \rangle = \frac{\pi^2 q^2 c_0^2 k_B T s b^4}{2 \nu \rho a^2} \sum_{n,m=1}^N K_n^{-1} K_m^{-1} R_{nm}$$

$$R_{nm} = \int_0^{\infty} \frac{\cos \tilde{k} \left(\frac{\tilde{a}}{2} + \tilde{\xi}_n \right) d\tilde{k}}{\tilde{\lambda} \sinh \tilde{\lambda} \tilde{d} \sinh \tilde{k} \tilde{d}} \int_0^{\infty} \frac{\cos \tilde{k} \left(\frac{\tilde{a}}{2} + \tilde{\xi}_m \right) \left(G(\tilde{k}, \tilde{k}_1) - \frac{3}{\tilde{d}} F(\tilde{k}, \tilde{k}_1) \right) d\tilde{k}_1}{\tilde{\lambda}_1 \sinh \tilde{\lambda}_1 \tilde{d} \sinh \tilde{k}_1 \tilde{d}} \times$$

$$\times \int_{S_{el}} \tilde{j}_0(\tilde{x}) \sin \tilde{k} \tilde{x} d\tilde{x} \int_{S_{el}} \tilde{j}_0(\tilde{x}_1) \sin \tilde{k}_1 \tilde{x}_1 d\tilde{x}_1$$

$$G(\tilde{k}, \tilde{k}_1) = g(\tilde{k} + \tilde{\lambda}, \tilde{k}_1 + \tilde{\lambda}_1) + g(\tilde{k} + \tilde{\lambda}, \tilde{\lambda}_1 - \tilde{k}_1) +$$

$$+ g(\tilde{\lambda} - \tilde{k}, \tilde{k}_1 + \tilde{\lambda}_1) + g(\tilde{\lambda} - \tilde{k}, \tilde{\lambda}_1 - \tilde{k}_1)$$

$$g(\varphi, \psi) = \frac{\sinh \tilde{d}(\varphi + \psi)}{\varphi \psi (\varphi + \psi)} - \frac{\sinh \tilde{d}(\varphi - \psi)}{\varphi \psi (\varphi - \psi)} - \frac{(\cosh \tilde{d}\varphi - 1)(\cosh \tilde{d}\psi - 1)}{\tilde{d}\varphi^2 \psi^2}$$

$$F(\tilde{k}, \tilde{k}_1) = (g(\tilde{\lambda} + \tilde{k}) + g(\tilde{\lambda} - \tilde{k})) (g(\tilde{\lambda}_1 + \tilde{k}_1) + g(\tilde{\lambda}_1 - \tilde{k}_1))$$

$$g(\varphi) = (\cosh(\varphi \tilde{d}) - 2 \sinh(\varphi \tilde{d}) / \varphi \tilde{d} + 1) / \varphi^2$$
(23)

Note that in the high frequency range, $\tilde{\lambda}, \tilde{\lambda}_1, \tilde{\lambda} - \tilde{k}, \tilde{\lambda}_1 - \tilde{k}_1$ can be replaced by $\sqrt{\tilde{\omega}}$, all the expressions containing the quotient of hyperbolic functions can be replaced by unity in the expressions (18) and (23). After such simplifications $R_{n,m} \sim \tilde{\omega}^{-5/2}, K_n^{-1}, K_m^{-1} \sim \tilde{\omega}^{1/2}$ and (23) can be approximated by power dependence $\langle I_{\omega}^2 \rangle \sim \tilde{\omega}^{-3/2}$.

3. Results and discussion

3.1. Calculations

The following parameters, corresponding to the experimental sample described above, have been used in numerical calculations based on the Eqs. (16)–(23): $\tilde{d} = 5$, $\tilde{a} = 1$. All the calculations, including inversion of the matrixes, have been performed in Matlab software. First, the stationary current density distribution across the cathode surface has been found from (17), (19) and the first equation of (16). The resulting curve is given in Fig. 7.

It can be seen from the presented graph that, as expected, the current density is maximum at the edge of the cathode facing the anode in the anode-cathode pair. Note that the value of the current at the opposite end of the electrode also exceeds the value at its center, which is due to the fact that in this area active ions diffuse not only from the region immediately above the cathode but

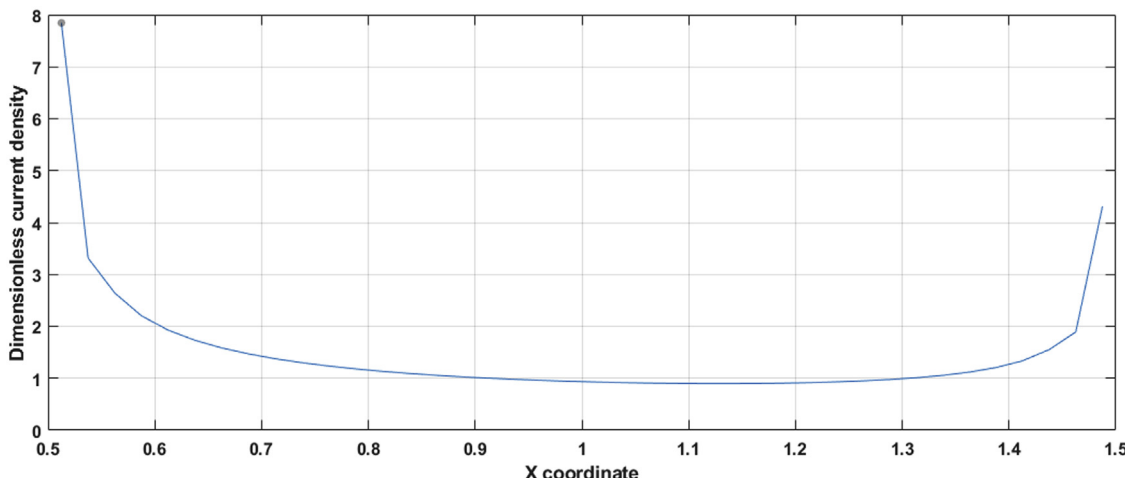


Fig. 7. Stationary current distributions over the cathode.

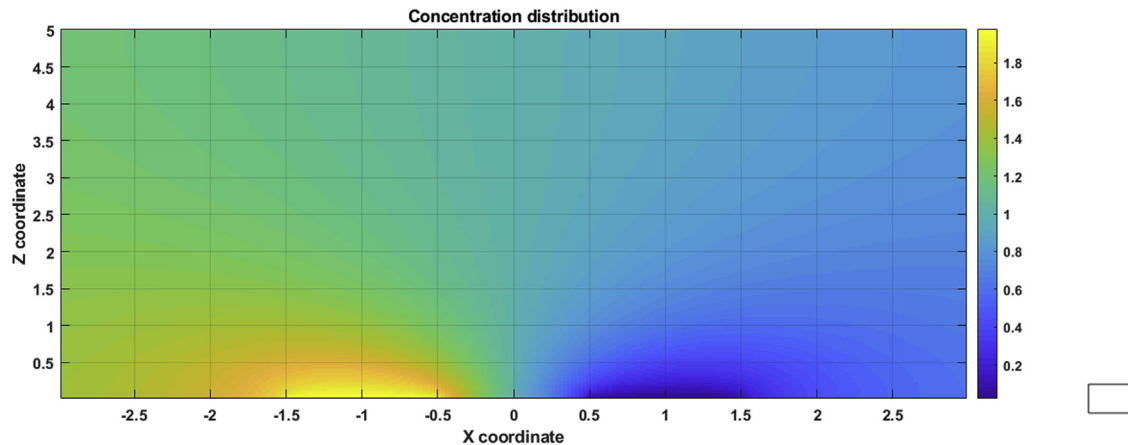


Fig. 8. Active ions stationary distributions in the electrochemical cell.

also from the space adjacent to the cathode. The distribution of the dimensionless concentration $\tilde{c} = c/c_0$ of active ions in the channel is shown in Fig. 8. The dark blue color corresponds to the zero concentration, which is achieved at the cathode at $0.5 < \tilde{x} < 1.5$.

While the stationary concentration distribution is known, the electrical current fluctuations have been found from (24) and (23). The frequency behavior of the dimensionless power spectral density is shown in Fig. 9.

It can be seen from the above graph that at low frequencies the spectral current density varies rather slowly, while at high frequencies it varies much faster and can be approximated by dependence $\sim 1/\tilde{\omega}^{1.5}$. Qualitatively, this behavior corresponds to the experimental data on the convective type noise measurements presented in [12], in spite of the different geometry of the studied converting cell.

3.2. Experiments

Before comparing the simulation result with the experimental data, note that the noise is generally caused by simultaneous contribution of several physical mechanisms, such as thermal noise, geometrical noise and noise of signal conditioning electronics [9] and [10]. At the same time, according to the experimental data from [12,13] and [14], convective noise is predominant in a significant part of the working frequency range (from 2 to 3 Hz to about 100 Hz). In this range, the comparison of model data for convective noise and experimentally measured noise is apparently legitimate. The coincidence of the experimentally measured noise with the simulation results for this frequency range will indicate the adequacy of the assumptions and the constructed model.

To experimentally measure the noise of the sensor with a planar cell, the sensor has been placed in a protective case preventing the occurrence of a spurious signal due to fluctuations in temperature and pressure throughout the experiment. It has been installed together with a reference device (seismometer CME6011 with sensitivity of 2000 V/m/s in a frequency range of 0.033–50 Hz) on a consolidated foundation located in a basement. The signals have been recorded for several hours during the night time and digitized using a high-resolution data acquisition system. The sensor signal density has been transformed into spectral density in units of acceleration by dividing the first by the frequency response function of the sensor (presented in Fig. 5) and multiplying it by the coefficient K_A :

$$a(\omega) = K_A \cdot I_{out}(\omega) / W_I(\omega) \quad (24)$$

The signals spectral densities are shown in Fig. 10. The spectral density of the studied sensor signal is shown in blue, the spectral density of the reference seismometer is shown in red for comparison. To calculate the noise spectral density of the sensor, the algorithm of estimating sensor self-noise compared to the reference device with known amplitude-frequency and noise parameters has been used [31] (shown in green in Fig. 10).

Regarding the planar cell as an input current noise source, the noise spectral density curve in electrical current units can be obtained by dividing the acceleration power spectral density of the sensor noise (green curve in Fig. 10) by experimentally measured squared frequency response function and coefficient K_A :

$$\langle I_N \rangle^2 = \langle a_N \rangle^2 |W_I(\omega)|^2 / K_A^2 \quad (25)$$

The dependence obtained in this way is shown in Fig. 11 (red curve).

To compare it with the results of the modeling, move to the dimensional values in the calculation results. To do this, it is sufficient to multiply the power spectral density of the dimensionless output shown in Fig. 9 by the factor $\frac{\pi^2 q^2 c_0^2 k_B T_{sh} b^4}{2v\rho l a^2}$ and go from dimensionless frequencies to frequencies expressed in Hz. In addition, the calculated value of the spectral density must be multiplied by 2 to take into account the presence of the second pair of electrodes in the experimental sample, which is symmetrically located. Use the following numerical values of the parameters of the transforming electrochemical cell: $c_0 = 0.01 \text{ mol/l}$, $T = 300 \text{ K}$, $s = 6 \text{ mm}$, $v = 10^{-6} \text{ m}^2/\text{s}$, $\rho = 1500 \text{ kg/m}^3$, $D = 2 \cdot 10^{-9} \text{ m}^2/\text{s}$, $b = 20 \text{ mkm}$, $l = 18 \text{ mm}$. The result of the calculation is shown in Fig. 11 by the blue curve.

The sensor current noise density curve in Fig. 11 aligns well with the theoretical dependence in the range of 2–200 Hz, which confirms the assumption of the convective nature of the planar cell noise in this frequency range. At lower frequencies, the observed experimental data differs markedly from the theoretical calculations. Apparently, this is due to the prevalence of other mechanisms of self-noise generation in this frequency range, which agrees with previously published empirical models and experimental data on various types of MET sensors self-noise [12–14].

3.3. Conclusions

To sum up, the novelty of the presented results lies in the fact that the theoretical description of the convective noise in electrochemical cell used as the conversion element of molecular electronic motion sensors confirmed by experimental data

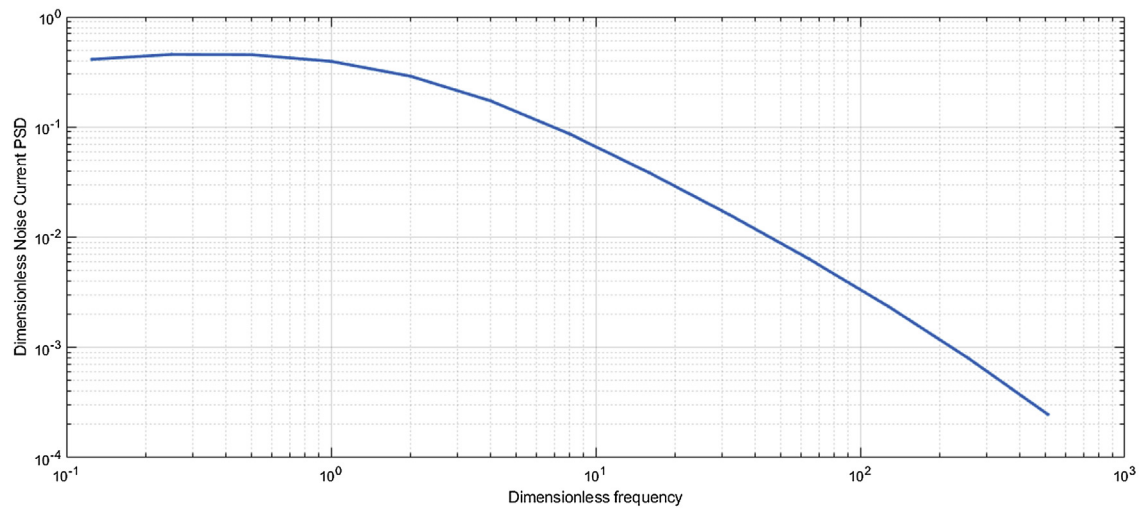


Fig. 9. Electrode current self-noise power spectral density.

dB rel. $1 \text{ m/s}^2/\sqrt{\text{Hz}}$)

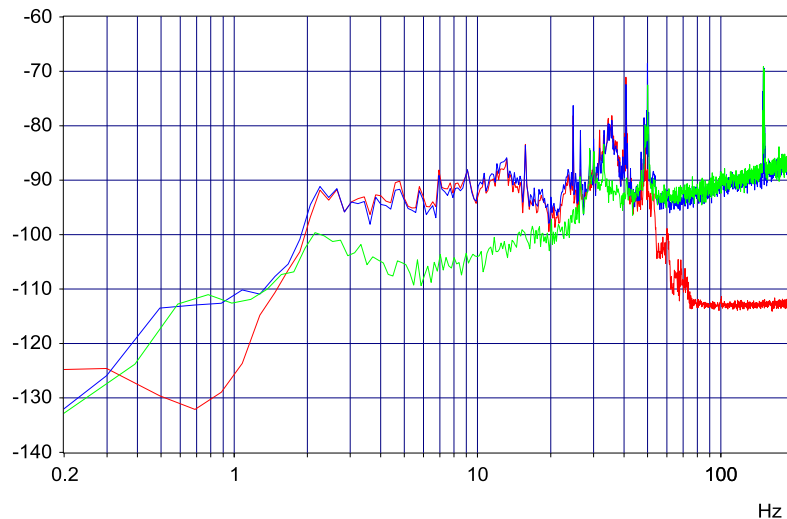


Fig. 10. The spectral density of the sensor signal with a planar cell (blue curve), of the reference device CME6011 (red curve), the noise component of the sensor signal with a planar cell (green curve). X-axis is shown in Hz, Y-axis is shown in dB relative to 1. (For interpretation of the references to colour in this figure legend, the reader is referred to the web version of this article). $\text{m/s}^2/\sqrt{\text{Hz}}$

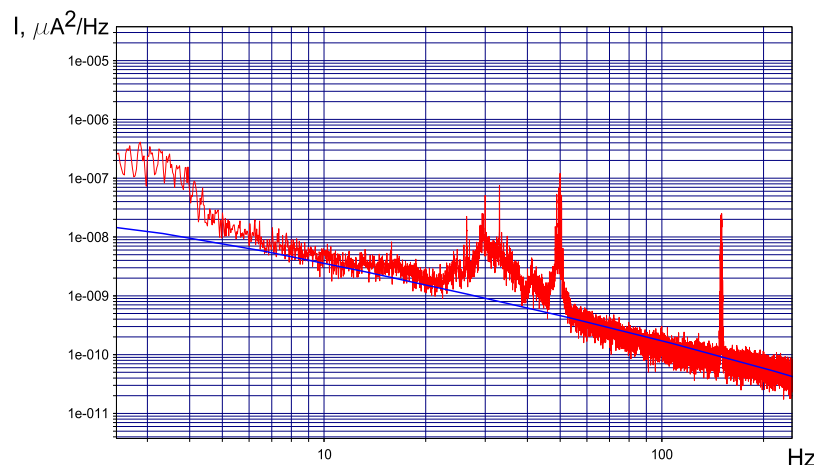


Fig. 11. The spectral density of the noise current (red curve) and a straight line of reference of the frequency dependence by the law of $1/f^{1.5}$ (blue curve). X-axis is shown in Hz. (For interpretation of the references to colour in this figure legend, the reader is referred to the web version of this article).

is suggested. The theoretical model is based on the hypothesis that convective noise is conditioned by non-uniform variations of hydrodynamic flows in the electrolyte, which are related to the influence of random local forces. Mathematically, the stochastic flows are described by the Navier-Stokes equation with a random force in the right-hand side, where the mean value is zero and the correlation properties are described by the Eq. (9) [21].

For the studied planar geometry of the electrochemical cell electrodes, the initial system of equations can be reduced to integral equations to calculate the electric current – both steady and alternating. The result of the calculations is the frequency dependence of the PSD of the electric current fluctuations.

The electrochemical cells samples and seismic sensors based on them have been produced. The cells geometry has corresponded to the parameters used in the calculations. The experimental curves the noise of the electrochemical cell output current have been measured and have proved to be in good agreement with the theoretical data.

The good agreement between the experimental data and the modeling results can be regarded as proof of the validity of the assumed hypothesis about the nature of the studied type of noise.

Acknowledgements

The authors acknowledge Russian Ministry of Education and Science for the support; the project ID is RFMEFI57817X0243.

References

- [1] V. Agafonov, A. Neeshpapa, A. Shabalina, Electrochemical seismometers of linear and angular motion, in: M. Beer, I.A. Kougioumtzoglou, E. Patelli, I.S.-K. Au (Eds.), Encyclopedia of Earthquake Engineering SE - 403-1, Springer Berlin Heidelberg, 2015, pp. 944–961.
- [2] F. Bernauer, J. Wassermann, H. Igel, Rotational sensors-a comparison of different sensor types, *J. Seismol.* 16 (4) (2012) 595–602.
- [3] A.T.J. Makris, J. Papoulias, A real-time seismic and tsunami network in the Kyparissiakos Gulf, Greece, *Boll. di Geofis. Teor. ed Appl.* 55 (2014) 561–587, no. June.
- [4] I. Koulakov, et al., Asymmetric caldera-related structures in the area of the Avacha group of volcanoes in Kamchatka as revealed by ambient noise tomography and deep seismic sounding, *J. Volcanol. Geotherm. Res.* 285 (2014) 36–46.
- [5] D.G. Levchenko, I.P. Kuzin, M.V. Safonov, V.N. Sychikov, I.V. Ulomov, B.V. Kholopov, Experience in seismic signal recording using broadband electrochemical seismic sensors, *Seism. Instruments* 46 (3) (2010) 250–264.
- [6] N.K. Kapustian, G.N. Antonovskaya, V.M. Agafonov, K.A. Neumoin, Seismic monitoring of linear and rotational oscillations of the multistory buildings in Moscow, in: 6th European Workshop on Theseismic Behavior of Irregular and Complex Structures (GEWICS), September (12–13), 2011, pp. 1–9.
- [7] V.A. Kozlov, V.M. Agafonov, J. Bindler, A.V. Vishnyakov, Small, low-power, low-cost IMU for personal navigation and stabilization systems, *Proc. Inst. Navig. Natl. Tech. Meet.* 2 (2006) 650–655.
- [8] V.I. Gorbenko, R.A. Zhostkov, D.V. Likhodeev, D.A. Presnov, A.L. Sobisevich, Feasibility of using molecular-electronic seismometers in passive seismic prospecting: deep structure of the Kaluga ring structure from microseismic sounding, *Seism. Instruments* 53 (3) (2017) 181–191.
- [9] H. Huang, V. Agafonov, H. Yu, Molecular electric transducers as motion sensors: a review, *Sensors (Basel.)* 13 (4) (2013) 4581–4597, Jan.
- [10] B.M. Grafov, A.M. Kuznetsov, A.E. Sunsov, Fluctuation-dissipation analysis of diffusion and discharge processes, *J. Electroanal. Chem.* 533 (1–2) (2002) 19–23.
- [11] A.S. Bugaev, et al., Measuring devices based on molecular-electronic transducers, *J. Commun. Technol. Electron.* 63 (12) (2018) 1339–1351.
- [12] V.M. Agafonov, D.L. Zaitsev, Convective noise in molecular electronic transducers of diffusion type, *Tech. Phys.* 55 (1) (2010) 130–136, Jan.
- [13] I.V. Egorov, A.S. Shabalina, V.M. Agafonov, Design and self-noise of MET closed-loop seismic accelerometers, *IEEE Sens. J.* 17 (7) (2017) 2008–2014.
- [14] D. Zaitsev, V. Agafonov, E. Egorov, A. Antonov, A. Shabalina, Molecular electronic angular motion transducer broad band aelf-noise, *Sensors* 15 (11) (2019), Multidisciplinary Digital Publishing Institute, pp. 29378–29392, 20-Nov-2015.
- [15] D. Zaitsev, V. Agafonov, E. Egorov, S. Avdyukhina, Broadband MET hydrophone, EAGE Conference & Exhibition 2018, 11–14 June 2018 (2018).
- [16] V.G. Krishtop, V.M. Agafonov, A.S. Bugaev, Technological principles of motion parameter transducers based on mass and charge transport in electrochemical microsystems, *Russ. J. Electrochem.* 48 (7) (2012) 746–755.
- [17] J.-B. Wang, L.-M. Gong, D.-Y. Chen, W.-T. He, P. Wang, MEMS based electrochemical seismic sensors with planar electrodes, *Guangxue Jingmi Gongcheng/Optics Precis. Eng.* 23 (3) (2015).
- [18] F. Detcheverry, L. Bocquet, Thermal fluctuations of hydrodynamic flows in nanochannels, *Phys. Rev. E - Stat. Nonlinear, Soft Matter Phys.* 88 (1) (2013) 1–15.
- [19] L.D. Landau, L. E. M. Statistical physics part 2, in: *Statistical Physics Part 2*, Second, Pergamon Press, 1980, pp. 397.
- [20] M. Liang, H. Huang, V. Agafonov, R. Tang, R. Han, H. Yu, Molecular electronic transducer based planetary seismometer with new fabrication process, in: *Proceedings of the IEEE International Conference on Micro Electro Mechanical Systems (MEMS)*, 2016, 2016, pp. 986–989, Febru.
- [21] Z. Sun, D. Chen, J. Chen, T. Deng, G. Li, J. Wang, A Mems Based Electrochemical Seismometer With a Novel Integrated Sensing Unit, no. January, 2016, pp. 247–250.
- [22] T. Deng, D. Chen, J. Chen, Z. Sun, G. Li, J. Wang, Microelectromechanical systems-based electrochemical seismic sensors with insulating spacers integrated electrodes for planetary exploration, *IEEE Sens. J.* 16 (3) (2016) 650–653.
- [23] G. Li, et al., A flexible sensing unit manufacturing method of electrochemical seismic sensor, *Sensors* 18 (4) (2018) 1165.
- [24] L. Chen, Z. Sun, G. Li, D. Chen, J. Wang, J. Chen, A monolithic electrochemical micro seismic sensor capable of monitoring three-dimensional vibrations, *Sensors* 18 (4) (2018), 1047.
- [25] L. Bay, K. West, B. Winther-Jensen, T. Jacobsen, Electrochemical reaction rates in a dye-sensitised solar cell – the iodide/tri-iodide redox system, *Sol. Energy Mater. Sol. Cells* 90 (3) (2006) 341–351.
- [26] V.M. Volgin, A.D. Davydov, Mass-transfer problems in the electrochemical systems, *Russ. J. Electrochim.* 48 (6) (2012) 565–569.
- [27] D.A. Bograchev, A.D. Davydov, Theoretical study of the effect of electrochemical cell inclination on the limiting diffusion current, *Electrochim. Acta* 47 (20) (2002) 3277–3285.
- [28] V.M. Agafonov, E.V. Egorov, A.S. Bugaev, Application of the convective diffusion equation with potential-dependent boundary conditions to the charge transfer problem in four-electrode electrochemical cell on the condition of small hydrodynamic velocity, *Int. J. Electrochim. Sci.* 11 (2) (2016).
- [29] L.D. Landau, E.M. Lifshitz, Hydrodynamic fluctuations, *J. Exp. Theor. Phys.* 32 (1957) 618–619.
- [30] G. Grün, K. Mecke, M. Rauscher, Thin-film flow influenced by thermal noise, *J. Stat. Phys.* 122 (6) (2006) 1261–1291.
- [31] I. Tasić, F. Runovc, Seismometer self-noise estimation using a single reference instrument, *J. Seismol.* 16 (2) (2012) 183–194.

Biographies

Vadim M. Agafonov was born in Leningrad, Russia, in 1966. He received the M.S. degree in electronics and control systems and the Ph.D. degree in physics of dielectrics and semiconductors from the Department of Physical and Electronics, Moscow Institute of Physics and Technology, Dolgoprudny, Moscow, in 1989 and 1992, respectively. Since 1998, he has been an Associate Professor with the Department of Physical and Electronics, Moscow Institute of Physics and Technology (State University), and the Director of the Center for Molecular Electronics, Moscow Institute of Physics and Technology. His main interests include charge transfer in liquids and solid/liquid interfaces and the development of liquid-based motion sensors.

Anna S. Shabalina was born in Bryansk, Russia, in 1977. She received the B.S. and M.S. degrees in physical engineering from the Department of Physical and Quantum Electronics, Moscow Institute of Physics and Technology, in 2000. She has been a Research Engineer with the Center for Molecular Electronics, Moscow Institute of Physics and Technology, since 2000. She is the author of more than ten articles. Her research interests include seismic sensors development, impedance and noise measurements, and fundamental study of electrochemical cell.

Dongge Ma studied semiconductor device physics at Liaoning University and Jilin University (China), where he received his BSc in 1989 and PhD in 1995, respectively. After additional years as a visiting professor and research fellow in Universidade Federal do Paraná, Brazil, and Durham University and St. Andrews University, UK, he joined Changchun Institute of Applied Chemistry, CAS, as a professor in 2001. In 2016, he joined South China University of Technology. Now he is a group leader of organic optoelectronic device physics in State Key of Luminescent Materials and Devices in South China University of Technology. His research is focusing on the studies of organic optoelectronic devices, including white organic light-emitting diodes, organic photodetectors and organic lasers, and the physics processes in organic semiconductors. Up to now, he has published over 400 papers on organic electronics, and the cited numbers in published papers are over 10,000 times.

Vladimir G. Krishtop received the B.S. and M.S. degrees in applied mathematics and physics from the Moscow Institute of Physics and Technology (MIPT), in 1999 and 2001, respectively, and the Ph.D. degree in physical electronics in 2004. Since 2010, he has been a Researcher with the Institute of Microelectronics Technology and High- Purity Materials of the RAS (IHPM RAS). Since 1999, he has been an Engineer and/or Researcher with the Research Department, MIPT, Center for Molecular Electronics, MIPT, IHPM RAS, R-sensors LLC, JSC NPP Kvant (Open Joint-Stock Company Research-Production Enterprise Kvant), Fryasino Branch, IRE RAS. From

2002 to 2013, he was an Assistant Professor and then an Associate Professor with the Department of General Physics, MIPT, and Department of Molecular Electronics, MIPT. In 2013, he was an Associate Professor of Molecular Electronics. From 2002 to 2005, he was the Deputy Dean of the Department of Physical and Quantum Electronics, Moscow Institute of Physics and Technology. He has authored over 20 articles, and three patents. In 2012, he received a Medal and Prize from the Russian Academy of Sciences for Best Young Scientists of RAS in the field of the design and

development of devices, techniques, technologies and new scientific and technological products of scientific and applied significance. His research interests include microelectronic technologies, temperature effects and stability in electrochemical devices, developing devices based on a new physical principles, and hybrid devices that combined a modern achievements of microelectronics, microhydrodynamics, and electrochemistry.